Density-functional studies of tungsten trioxide, tungsten bronzes, and related systems

B. Ingham,[1] S. C. Hendy,[1,2] S. V. Chong,[2] and J. L. Tallon[1,2]
[1]*Victoria University of Wellington, P.O. Box 600, Wellington, New Zealand*
[2]*Industrial Research Ltd., P.O. Box 31310, Lower Hutt, New Zealand*
(Received 1 February 2005; revised manuscript received 13 June 2005; published 2 August 2005)

Tungsten trioxide adopts a variety of structures which can be intercalated with charged species to alter the electronic properties, thus forming "tungsten bronzes." Similar effects are observed upon removing oxygen from WO_3. We present a computational study of cubic and hexagonal alkali bronzes and examine the effects on cell size and band structure as the size of the intercalated ion is increased. With the exception of hydrogen (which is predicted to be unstable as an intercalate), the behavior of the bronzes are relatively consistent. $NaWO_3$ is the most stable of the cubic systems, although in the hexagonal system the larger ions are more stable. The band structures are identical, with the intercalated atom donating its single electron to the tungsten 5*d* valence band. A study of fractional doping in the Na_xWO_3 system ($0 \leqslant x \leqslant 1$) showed a linear variation in cell parameter and a systematic shift in the Fermi level into the conduction band. In the oxygen-deficient WO_{3-x} system the Fermi level undergoes a sudden jump into the conduction band at around $x=0.2$. Lastly, three compounds of a layered $WO_4 \cdot \alpha,\omega$-diaminoalkane hybrid series were studied and found to be insulating, with features in the band structure similar to those of the parent WO_3 compound that relate well to experimental UV-visible spectroscopy results.

DOI: 10.1103/PhysRevB.72.075109 PACS number(s): 71.15.Mb, 61.72.Ww, 71.20.Nr, 81.07.Pr

I. INTRODUCTION

Tungsten trioxide has long been studied for its interesting structural, electronic, and electrochromic properties. Tungsten trioxide is most stable in a pseudocubic, distorted ReO_3 structure[1] but can also form metastable hexagonal,[2] tetragonal,[3] and pyrochlore[4,5] structures. For all of these structures it is possible to intercalate monovalent or divalent cations in the interstices within the structures to form the so-called tungsten bronzes.[3,6–8] The resulting materials exhibit a continuous color change[9] and often a large increase in the electrical conductivity, which becomes metallic in nature.[10] The most-studied system is that of the cubic alkali bronzes (M_xWO_3, M=group I alkali ions, $0 \leqslant x \leqslant 1$). Of these, the sodium bronze is the only compound that has been reported with $x=1$;[9] however, in the hexagonal system, all alkali ions (Li–Cs) have been intercalated to varying degrees.[1] In the cubic system, even low levels of doping ($x < 0.2$) cause a dramatic color change, which has led to tungsten trioxide being used as a material in electrochromic windows.[11–13] Bulk superconductivity has been observed at 2–3 K in $Na_{0.2}WO_3$.[14] In addition to electronic doping, tungsten trioxide can also exhibit electron doping via the removal of oxygen, with similar coloration effects.[15] However, coloration and conduction are not strictly related, as the conductivity in a thin film of oxygen-deficient WO_{3-x} is much lower than in a thin film of M_xWO_3 of the same color.[16] This indicates that the mechanism for mobility is not simply due to delocalized electrons or holes, but rather changes in the band structure near the Fermi level, which are different for the two types of material.[16,17] Recent work by our group has concentrated on developing organic-inorganic hybrid materials based on two-dimensional tungsten oxide sheets (formed by corner-shared WO_6 octahedra) linked with organic diamine molecules.[18,19] These exhibit a great diversity of structure and present a model system with interesting low-dimensional properties. The electronic structure of these materials will determine how they may be used in various electronic applications. This work presents *ab initio* computations on a variety of tungsten oxide derivatives, including a series of cubic and hexagonal alkali tungsten bronzes, variable-doping Na_xWO_3 ($0 \leqslant x \leqslant 1$), oxygen-deficient WO_{3-x}, and some simple layered organic-inorganic tungsten oxide hybrid structures to aid in understanding the optical and electronic properties of the latter. A fuller version of this paper may be found in Ref. 20. While we were completing this work, another paper has appeared which treats some of the parent materials.[21]

II. COMPUTATIONAL DETAILS

We have applied density-functional theory (DFT) within the generalized gradient approximation[22] (GGA) using the VASP package,[23–26] which solves the DFT-GGA Kohn-Sham equations within the pseudopotential approximation. Here the valence electrons have been expanded in a plane-wave basis set and the effect of the core on the valence electrons has been modeled with ultrasoft pseudopotentials. We used ultrasoft Vanderbilt-type pseudopotentials[27] as supplied by Kresse and Hafner.[28] The pseudopotential valence states used are as follows: W, $6s^15d^5$; O, $2s^22p^4$; H, $1s^1$; Li, $2s^1$; Na, $3s^1$; K, $4s^1$; Rb, $5s^1$; Cs, $6s^1$; C, $2s^22p^2$; N, $2s^22p^3$. In all the calculations here, we used a plane-wave cutoff of 396 eV.

To study the effect of fractional doping in the Na_xWO_3 system, we used a supercell method consisting of up to eight primitive WO_3 cells, with between 1–7 of these cells occupied by sodium ions in a pseudorandom fashion. Similarly for the oxygen-deficient WO_{3-x} system, 3–6 cells were used with one oxygen vacancy in each case. In all cases the basis

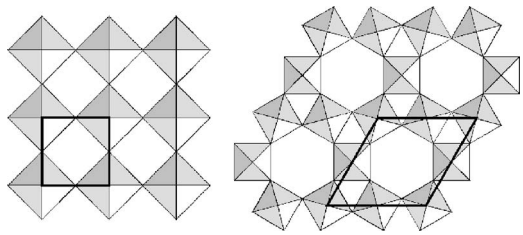

FIG. 1. The structure of cubic (left) and hexagonal (right) tungsten oxide and bronzes. The unit cell is indicated in each case.

vectors of the cell were chosen to avoid the creation of lines or planes of dopants.

k-point meshes between $4\times4\times4$ and $15\times15\times15$ were used to relax the various systems, corresponding, respectively, to 24–36 and 120–455 *k* points in the irreducible Brillouin zone. In all cases the *k*-point mesh was varied at the end of the relaxation, and the energy was found to converge to better than 10 meV. The cell parameters and atomic positions were allowed to relax in alternate cycles, because of instability in the calculations, especially for the hybrid structures. The atomic positions were considered relaxed when the total energy had converged to within 10 meV between ionic steps. In the calculations of the hybrid structures, the relative positions of the in-plane tungsten and oxygen atoms were fixed at the origin and halfway along each planar axis, respectively—again, to avoid instability in the calculations.

Finally we note that with the exception of the oxygen-molecule total energy, none of the calculations here were spin polarized. The total energy of the oxygen molecule in its ${}^3\epsilon_g^-$ ground state, used to compute energies of formation for the WO_{3-x} series, was computed in a 16 Å cubic cell with convergence of the energy to within 10 meV. Our binding energy for the oxygen molecule of 3.214 eV/atom is consistent with other calculated values reported in the literature.[29]

III. CUBIC AND HEXAGONAL ALKALI BRONZES

A. Structure

The group I elements (H, Li, Na, K, Rb, and Cs) were each used as the intercalated species in cubic $M\mathrm{WO}_3$ ($x=1$ bronzes) and hexagonal $M_{0.33}\mathrm{WO}_3$ (full intercalation of the hexagonal tunnels). In each case the intercalated metal atom was placed in the plane of the apical oxygen atoms, in the center of the cavity (Fig. 1). WO_3 does not form a perfectly cubic cell at room temperature, as the WO_6 octahedra are slightly distorted in terms of W-O bond lengths and W-O-W bond angles, due to antiferroelectric displacement of the tungsten atoms and subsequent rotation of the WO_6 octahedra.[1,30] However, this was not observed in the current calculated system, as the cell always relaxed to a cubic structure. In calculations involving supercells of tungsten trioxide, the distortions are seen.[21] Tungsten bronzes, on the other hand, do form the simple cubic structure at high-intercalation levels.[31] The hexagonal structure, which was also studied for comparison, is the same for both the oxide and bronzes. (The term "cubic" is used connotatively throughout this paper for those systems that are cubic or close to it, as opposed to the hexagonal systems also studied.)

Table I shows some experimental results for the cubic bronze system. In the case of pseudocubic WO_3, a cubic cell was calculated from the volume average of the given parameters. Experimentally, only sodium is able to form a stable structure with $x=1$ at normal temperatures and pressures. In general the calculated cell parameters for the cubic system are larger than the experimental. It is also noticeable that as the size of the intercalated ion increases, the cell size increases dramatically. The Goldschmidt tolerance factor for cubic perovskites can be calculated from the formula

$$t=\frac{r_M+r_O}{\sqrt{2}(r_W+R_O)}$$

where r_j are the ionic radii.[32] For a perovskite structure to be stable, t must be less than unity. The tolerance factors for $NaWO_3$ and KWO_3 are 0.909 and 1.056, respectively, indicating that the potassium atom is slightly too large to form a stable structure. Potassium cubic bronzes have been formed with high x contents, but only under high-pressure synthesis conditions.[33] Rubidium and caesium cubic bronzes with high x content cannot be formed. The hexagonal structure, having larger tunnels, is able to accommodate larger ions than observed in the cubic system. In the experimental system the

TABLE I. Experimental cell parameters for tungsten oxide and bronzes (from Refs. 1, 3, 31, and 33–35) compared with our calculated results for completely occupied tungsten bronzes.

	Cubic a (Å)		Hexagonal a (Å)		Hexagonal c (Å)	
	Experimental	Calculated	Experimental	Calculated	Experimental	Calculated
WO_3	3.8144	3.74	7.298	7.4103	3.899	3.8144
H_xWO_3[a]	3.8235[b]	3.75	7.38	7.4173	3.78	3.8111
Li_xWO_3	3.8712		7.405	7.4007	3.777	3.8219
Na_xWO_3	3.8911	3.8622	7.38	7.4034	3.775	3.8248
K_xWO_3	3.9375	3.9484[b]	7.37	7.4010	3.77	3.8282
Rb_xWO_3	3.9818		7.38	7.4163	3.78	3.8289
Cs_xWO_3	4.0409		7.38	7.4507	3.785	3.8342

[a]$x=1$ for cubic; $x=0.33$ for hexagonal.
[b]Extrapolated from $x<1$ values.

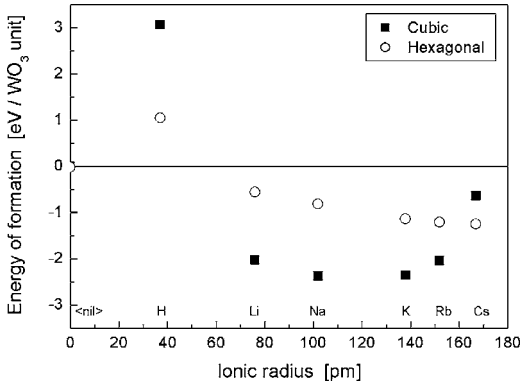

FIG. 2. Calculated energies of formation per WO_3 unit for cubic and hexagonal tungsten bronzes, relative to cubic WO_3.

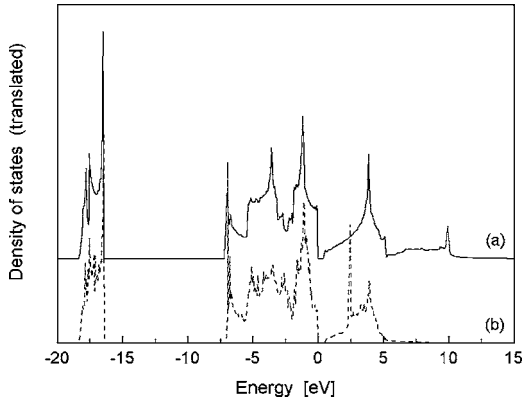

FIG. 3. The density of states as calculated for cubic (a) and hexagonal (b) WO_3.

stability of hydrogen is notoriously difficult to maintain, as it is quite mobile due to its small size. Both hydrogen and lithium are small enough ions to be able to also occupy the small triangular sites between the hexagonal tunnels.[1] Thus reported experimental results for H^+- and Li^+-hexagonal bronzes may show differing behavior from larger atoms because the occupied sites may be different in each case. In the experimental hexagonal system, the *a* parameter is observed to increase as ions are intercalated, while the *c* parameter decreases. The final values are relatively consistent across the series, as given in Table I. These are generally lower than the calculated values we have obtained, although most discrepancies are less than 0.5%.

For the hexagonal system, the changes in the lattice parameters are much less pronounced than in the cubic system, as shown in Table I. This is due to the hexagonal tunnel spaces being much larger than the cavities in the cubic system, and so the interactions between the inserted ion and the WO_3 lattice are smaller.

B. Charge density

Charge-density plots of the cubic and hexagonal systems (see Ref. 20) reveal that hydrogen behaves differently from the other intercalates. The single *s*-valence electron of the alkali ions is stripped from the intercalated atom, and only in the case of hydrogen is some charge still associated with the intercalate. That larger atoms are completely ionized is consistent with other reported experimental results.[30] It is interesting that the same phenomenon occurs in both the cubic and hexagonal cases. The first ionization energy of the intercalates are as follows: hydrogen 1.318 eV, lithium 0.526 eV, sodium 0.502 eV, potassium 0.425 eV, rubidium 0.409 eV, caesium 0.382 eV.[36] The high ionization energy of hydrogen with respect to the other intercalates may be responsible for the differing behavior.

C. Energies of formation

The energies of formation of the cubic and hexagonal tungsten bronzes are shown Fig. 2. These are calculated by subtracting the ground-state energies of the components (WO_3 plus the metal cation) from the ground-state energy of the final product (tungsten bronze). A negative energy of formation therefore indicates that the compound formed is stable.

Firstly, a comparison of cubic and hexagonal WO_3 shows that the hexagonal phase has a very similar energy to the cubic phase. Literature results indicate that the cubic phase is preferred, although the hexagonal phase is stable up to temperatures of 400–500 °C, indicating that the phase transition has a high activation energy.[1,2] In both the cubic and hexagonal systems, the hydrogen-intercalated bronze energy is positive and large, indicating that the hydrogen bronzes are not stable. Experimentally, the hydrogen bronzes are easily oxidized as the protons are highly mobile.[35,37] This result also relates to hydrogen being the only intercalate that does not ionize in the bronze structures, as evidenced by the charge density. For the hexagonal bronzes (apart from hydrogen) we find that there is a steady trend toward greater stability as the size of the intercalated alkali-metal ion increases, which is also indicated in the literature.[3] In the cubic system, however, the energy drops to a point and then, beyond Na, increases in the case of the larger intercalates. This point coincides with the stability limit predicted by the Goldschmidt perovskite-tolerance factor. For the stable compounds (WO_3, $LiWO_3$, and $NaWO_3$) there is a progressive decrease in the energy of formation. This supports experimental evidence that sodium may well be the most stable of the cubic bronzes, as it is the only one for which a fully intercalated compound has been reported.[37]

D. Density of states

For both the cubic and hexagonal systems other than hydrogen, the basic band structures of the bronzes are essentially identical to the parent oxide of the same phase. The only difference among them is the position of the Fermi level relative to the valence and conduction bands, which will be discussed later. Hence comparing the band structure of hexagonal and cubic WO_3 will aid a great deal in describing the bronze systems. A comparison of the density of states for cubic and hexagonal WO_3 is shown in Fig. 3. The lowest band, situated at −18 to −16 eV in all of the tungsten oxide-based systems studied to date, corresponds to the oxygen 2*s* orbitals.

The broad valence band, from −7 to 0 eV, is comprised mainly of oxygen 2*p* orbitals. There is a small tungsten 5*d* component, but this is negligible above −2 eV. The valence band cutoff is sharp at 0 eV and coincides in both the cubic and hexagonal case with the Fermi level, rendering the oxide materials semiconducting. The conduction band lies from 0.5 to 5 eV in both the cubic and hexagonal cases. In the cubic case it is solely comprised of tungsten 5*d* orbitals; however, in the hexagonal case there is also some additional oxygen 2*p* contribution—particularly to the strong peak feature observed at 2.5 eV. The band gaps are 0.4 eV in the cubic system and 0.5 eV in the hexagonal. These are much less than the experimentally observed band gap, which is typically reported in the range of 2.5–3 eV, and as being indirect[12,38,39] (which may lead to the large discrepancy). However, this is not too surprising, as DFT generally underestimates band gaps.

It is worth taking pause here to point out the similarities between this work and that of experimental results and other calculations reported on the same structures. X-ray photon spectroscopy (XPS) reveals that the valence band is comprised of oxygen 2*p* states only, and the conduction band of tungsten 5*d* states.[12,40] The oxygen 2*s* state at ~−20 eV has also been observed by XPS,[41] although given the precision of the measurement, this band is broadened out and appears to extend into the oxygen 2*p* valence band, the distinction of which is not made by the authors. Calculations using the local-density approximation and full-potential linear muffin-tin orbitals (where all electrons are considered, not just the valence electrons, as in the case of the VASP program) result in density-of-states spectra which are virtually identical to those we have obtained.[42,43] This is the case in both the cubic and hexagonal systems. An older paper by Bullet,[30] utilizing a nonrelativistic atomic orbital-based method, shows a very similar band structure (oxygen 2*p* as valence band and tungsten 5*d* as conduction band).

Figure 4 shows a comparison of the density of states of the cubic bronzes with the parent oxide. The hydrogen bronze system shows a large peak feature at the bottom of the conduction band, which is attributed to the nonionized hydrogen 1*s* orbital. Because only one electron is contributed from the hydrogen, the Fermi level lies near the middle of this subband. For the other bronze systems, analysis of the density-of-states contribution from each atom reveals that the intercalated atom contributes very little if at all to the overall density of states. This is expected due to its complete ionization, as the single valence electron of the intercalated atom is contributed to the W-O framework.[30] All compounds have the Fermi level located well into the conduction band, rendering them metallic. The shape of the band structure does not change as atoms are intercalated. This is also noted in other literature.[42,43] Also, the size of the band gap and the position of the Fermi level is relatively constant—even for those compounds which are known to be unstable (cubic potassium, rubidium, and caesium bronzes).

We have also derived the band structure curves along lines of symmetry in cubic WO_3 and cubic $NaWO_3$. The results appear virtually identical to the calculated band structures of both Bullett[30] and Cora *et al.*,[43] even though different methods were used for each calculation. Again, there is a high degree of similarity between the parent oxide and the sodium bronze, with the only major difference being the position of the Fermi level.

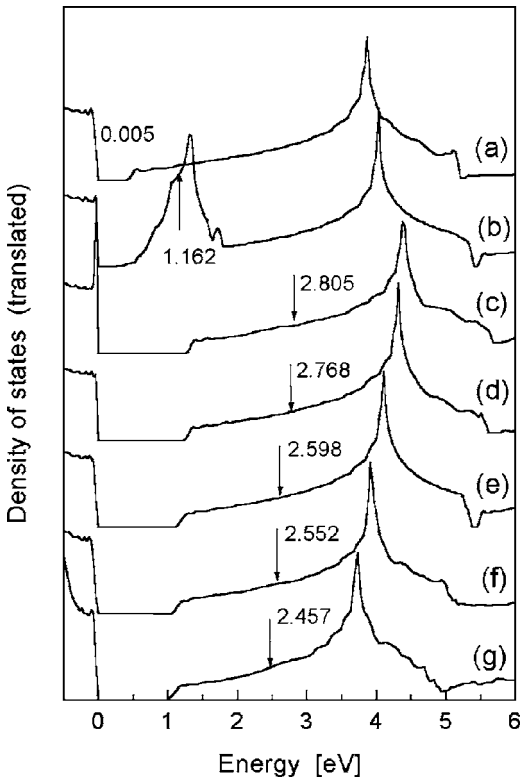

FIG. 4. Calculated density of states for cubic tungsten bronzes, MWO_3, near the Fermi level: (a) WO_3, (b) HWO_3, (c) $LiWO_3$, (d) $NaWO_3$, (e) KWO_3, (f) $RbWO_3$, (g) $CsWO_3$. The Fermi level is indicated in each case.

IV. CUBIC SODIUM TUNGSTEN BRONZE SERIES

Following the work comparing cubic and hexagonal tungsten bronzes, we set out to explore the sodium bronze system more thoroughly. Experimentally it is quite difficult to obtain a completely saturated sodium tungsten bronze (i.e., $x=1$).[31] There is a raft of experimental results, however, on sodium bronzes with $x<1$ (Refs. 3, 9, 10, 31, and 44, to name but a few), all illustrating that x is a continuous quantity. In addition to $x=0$ and 1, which were performed as part of the cubic tungsten oxide and alkali bronze series, we have calculated the structure and density of states for $x=n/8; n=1-8$. The average cubic cell parameter was found to increase linearly with x, as shown in Fig. 5(a). Also shown in this figure is a series of reported experimental results. At high x contents the agreement is very good. The discrepancy below $x=0.3$ is due to a phase change to a tetragonal form at low x values in the experimental system.[45] The structure of the tetragonal phase is a distorted version of the cubic phase.[3] As for the undoped WO_3 system, such distortions are not accounted for in the current calculations. In the work of Walkingshaw *et al.*[21] the volume versus x deviates from this linear behavior for x as large as 0.5.

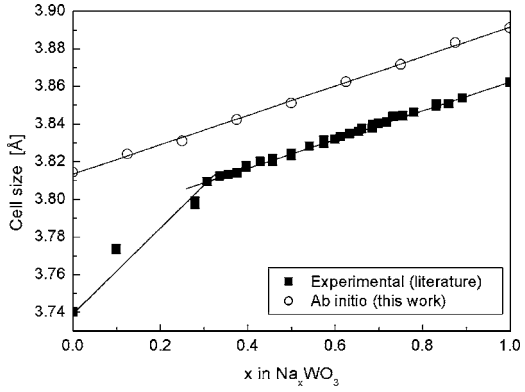

FIG. 5. (a) Calculated and experimental values of the cell parameter for cubic Na_xWO_3 with variable x. (b) Band gap and Fermi level of Na_xWO_3. The lines are given as a guide.

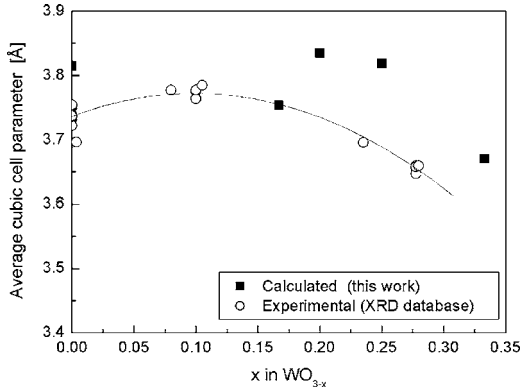

FIG. 6. The volume-averaged cubic cell parameter for calculated and experimental substoichiometric "cubic" WO_{3-x} systems. The curve is given as a guide.

The doping dependence of the band gap and Fermi level are shown in Fig. 5(b). The band gap increases linearly with x, while the Fermi level quickly moves up into the conduction band. According to this plot we would expect to see a semiconductor-metal transition at about $x=0.06$. However, in the experimental system this transition is observed at $x=0.3$, corresponding to (and perhaps influenced by) the structural transition (see Ref. 3, and references therein).

V. SUBSTOICHIOMETRIC WO_{3-x} SERIES

As a complement to the sodium bronze series, substoichiometric WO_{3-x} was examined for compounds with x ranging from zero to 0.33. In the experimental system, the maximum oxygen loss that can be achieved without a drastic phase change is ~0.35 (Ref. 46, and references therein). The oxygen composition is not continuous but "stages" to form different integral stoichiometric formulas for compounds in the range $WO_{2.65}$–WO_3. For all of these the crystal structure has been solved. They are given the names α-, β-, and γ-phase, and have been assigned the stoichiometries $WO_3(\alpha)$, $W_{20}O_{58}(\beta)$, and $W_{18}O_{59}(\gamma)$. The crystal structures of the β- and γ-phases were solved by Magneli.[47,48] Booth *et al.* generalize the β-phase even further by describing the existence of crystallographic shear planes.[49] This can account for the broad range of compositional formulas. While we are unable to calculate the properties of these exact phases as described in the literature, due to the restriction on the number of atoms in the system, we are able to observe the effect that removal of oxygen has on the simple cubic WO_3 phase.

As one might expect, removing oxygen from a site causes a local distortion of atoms around the vacancy, and the cell ceases to be simple orthorhombic. The cell volume changes; initially there is a slight increase at low deficiencies, followed by a decrease. These results are shown in Fig. 6 and are in good agreement with experimental values, despite the absence of the phase change in the calculated system.

The energies of formation for the different species studied are given in Table II. We note that a slight deficit of oxygen $\left(x=\frac{1}{6}\right)$ is more favorable energetically than stoichiometric WO_3. This is observed experimentally, as commercial WO_3 powder exhibits a loss of oxygen over 1–2 days in atmospheric conditions. Further loss of oxygen renders WO_{3-x} less energetically favorable than its parent oxide, and once again, as was the case with sodium tungsten bronzes, the presence of a phase change in the experimental system may explain any discrepancies seen.

It is also of interest to look at the changes in the density of states as oxygen is removed from WO_3. As mentioned in the Introduction, oxygen-deficient WO_3 exhibits an increased conductivity, but not as great as that due solely to the presence of doped electrons. Figure 7 shows the density of states for the WO_{3-x} system in the region near the Fermi level. The overall spectra share the same features previously detailed for WO_3: the oxygen 2s band near −18 eV; the broad valence band, comprised mainly of oxygen 2p orbitals, from −7 to 0 eV; and the conduction band, consisting solely of tungsten 5d orbitals, lying from roughly 0.5 to 5 eV. Naturally the substoichiometric systems appear more "jagged" than the parent WO_3 compound, due in part to the breaking of symmetry, rendering each atom nonequivalent to others within the cell and causing its contribution to be slightly different.

The inset in Fig. 7 shows the progression of the Fermi level into the conduction band. There is a sharp jump between $x=0.167$ and 0.2 as the Fermi level moves up into the conduction band—not a gradual transition as in the case of the sodium bronzes Na_xWO_3. While the $x=0.167$ compound has the Fermi level at zero (and therefore, still nonconducting), the band structure has already altered markedly. It ap-

TABLE II. Energies of formation of the calculated WO_{3-x} species calculated by the formula $E_F=E_{total}-\Sigma E_{parts}=E(WO_{3-x})-[E(WO_3)-(x/2)E(O_2)]$.

Formula	Energy of formation (eV/unit formula)
WO_3 $(x=0)$	0.0
$WO_{2.833}$ $\left(x=\frac{1}{6}\right)$	−0.028
$WO_{2.8}$ $\left(x=\frac{1}{5}\right)$	0.568
$WO_{2.75}$ $\left(x=\frac{1}{4}\right)$	1.120
$WO_{2.667}$ $\left(x=\frac{1}{3}\right)$	1.812

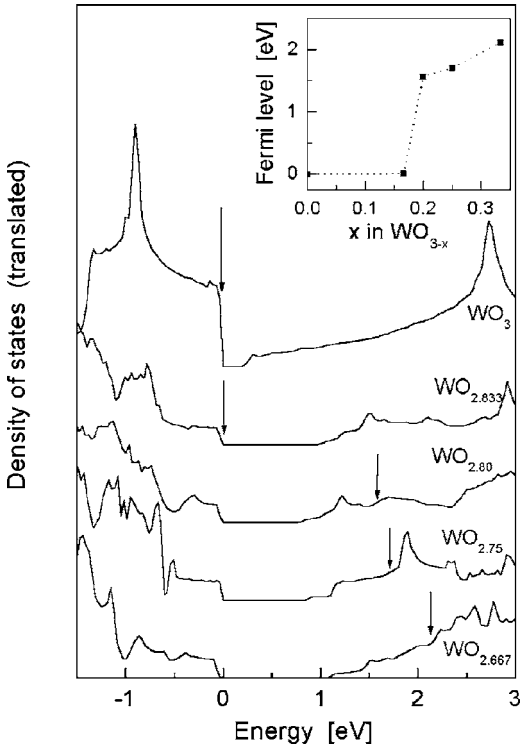

FIG. 7. Density of states for the WO_{3-x} system, all with the valence band set at zero. Arrows show the position of the Fermi level. Inset: Position of the Fermi level relative to the top of the valence band.

pears that there is a decrease in the density of states in the valence band, followed by the Fermi level being pushed up into the conduction band, while the band gap has increased significantly. The stoichiometry at which this insulating-conducting transition occurs is in good agreement with the literature value of $WO_{2.76}$, which coincides with the β-γ structural phase transition.[17]

An interesting future extension would be to examine the charge density of the WO_{3-x} structures and determine where the excess electrons are located, either on the now-vacant oxygen site or on the tungsten atoms on either side of the vacancy. Spin-polarized DFT calculations would also yield extra information about the changes in band structure observed near the Fermi level.

VI. ORGANIC-INORGANIC LAYERED HYBRIDS

Following on from the background studies of tungsten bronzes and the oxygen-deficient tungsten oxides, layered organic-inorganic hybrid compounds were studied to examine their electronic properties and compare these with the parent WO_3 compound. In fact this novel class of material is the primary object of our wider research.[18] They exhibit a diverse range of structure and physical properties and their ability to self-assemble at room temperature makes them attractive for a variety of potential applications. The materials as-prepared are expected to be semiconducting, but with doping it is hoped that conduction can be induced within the tungsten oxide planes.

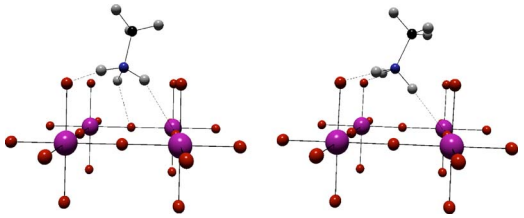

FIG. 8. (Color online) Calculated structure of methylamine in bridging (left) and apical (right) configurations.

The hybrid structure consists of WO_4 layers (as in H_2WO_4),[50] connected via aliphatic (linear) alkyl diamines. These have been investigated experimentally by us elsewhere.[18] Three different-length alkyl amines were used in the calculations, with two, four, and six carbons. The input structure of the hybrid systems is the most conceptually simple: a single unit formula, $WO_4 \cdot H_3N(CH_2)_nNH_3$ ($n=2,4,6$—hereby abbreviated as W-DAn). It is highly conceivable that the calculated structure of the hybrid compounds is in a slightly higher energy state than that of the actual structure, which may be a supercell of the simple input case, with possible tilts and rotations of the organic molecules and the WO_6 octahedra (as observed in WO_3). In extending the computations to the organic-inorganic systems then, several constraints were necessary. Firstly only one cell was used, which may affect the outcome not only due to the removal of distortion in the inorganic layer (which apparently lowers the energy in the oxide and hydrate compounds) but also because this does not allow for the differing orientation of the organic molecules in neighboring cells. Secondly, constraints were placed on the inorganic atoms in order to maintain the position of the layer. This entailed fixing the position of the tungsten and planar oxygen atoms at the corner and edges of the cell, respectively. This was sufficient to relax the atoms to a sensible structure.

These compounds are isostructural with diaminoalkane metal halides, which have been investigated by Mitzi.[51] There, two schemes were identified for the bonding of the organic ammonium group to the inorganic layer, designated "bridging" and "terminal" (which we shall call "apical").

The organic ammonium ($-NH_3^+$) terminal group forms hydrogen bonds to two bridging or two apical atoms (hence the designation "bridging" and "apical"), causing the alkyl chain to lie diagonally or parallel, respectively, within the cell. When the alkyl chain is longer than one carbon (methylamine), the second carbon in the chain would be too close to the opposing apical (oxygen) atom if a bridging conformation were adopted. Thus, in general, apical bonding is observed for organic-inorganic systems with organic chain lengths of two or more carbon atoms.

Given this, calculations were initially performed on the methylamine system in both the bridging and apical configurations, to compare the energies of each and as a starting point to construct the initial cells for the computations of the longer-chain diamine hybrids. Figure 8 shows the calculated relaxed structures of one methylammonium ion with respect to the tungsten oxide layer. In each case the orientation of the molecule within the cell is clearly shown, although for the bridging case it appears that there is a more delocalized at-

TABLE III. Calculated cell parameters of W-DA2 with the organic molecule in the bridging and apical conformations.

	W-DA2 bridging	W-DA2 apical
a (Å)	3.9443	3.9108
b (Å)	8.7345	8.7992
c (Å)	3.9443	3.9245
α	89.98	89.99
β	90.02	90.01
γ	90.02	90.01
Volume (Å^3)	135.8266	135.0498

traction between the hydrogen and oxygen atoms.

The apical configuration was determined to be more stable, as its energy was calculated to be 0.23 eV lower than that of the bridging structure. Each of the two methylamine structures were then used as the basis for the initial positions of the diaminoethane (DA2) compound. The relaxed cell parameters are given in Table III. In the apical case the cell volume is slightly less than in the bridging case. The two structures are shown in Fig. 9. Like the methylammonium structures, in the bridging conformation there are several longer bond distances from each hydrogen to the oxygen atoms, whereas in the apical conformation for each hydrogen there is a single bond that is distinctly shorter to one oxygen than the others.

The apical conformation has a calculated energy that is 1.04 eV lower than that of the bridging conformation, therefore rendering the apical form more stable, and indeed, the bridging structure has a negative cohesive energy. Two other systems were extended from the apical W-DA2: W-DA4 (4-carbon chain) and W-DA6 (6-carbon chain). Again the relative coordinates of the planar tungsten and oxygen atoms were fixed. The energies of formation were found to be as follows: W-DA2 −0.939 eV; W-DA4, −0.044 eV; W-DA6, −0.534 eV. From the negative values we conclude that all three compounds are stable, with W-DA4 being the least stable of the three (although the absolute ground-state energies are no doubt lower than these, due to the restrictions placed on the tungsten and oxygen atoms). This seems to be confirmed experimentally, as W-DA4 is harder to form than both W-DA2 and W-DA6.

The density of states of the three compounds are all very similar. The results are shown in Fig. 10. The main features

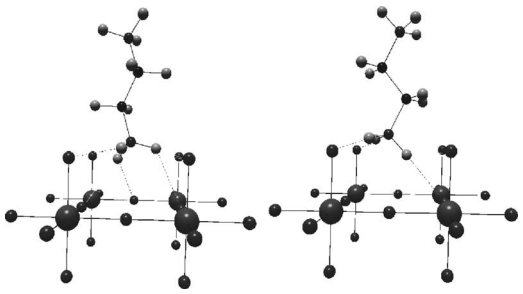

FIG. 9. Calculated structures of diaminoethane (DA2) in bridging (left) and apical (right) configurations.

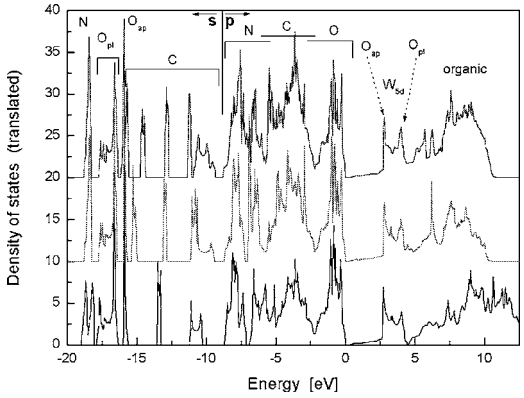

FIG. 10. Calculated density of states for W-DA2 (bottom), W-DA4 (middle), and W-DA6 (top). The Fermi level is located at $E=0$.

are as follows: As in the tungsten oxide and tungsten bronze systems, the oxygen $2s$ band is located between −18 and −16 eV. There is a splitting between the planar and apical oxygen contributions, with the planar oxygen bands being broader and lying at slightly lower energies. The nitrogen $2s$ bands lie at about −18.5 eV and the carbon $2s$ bands lie between −16 and −9 eV. The appearance of multiple carbon s bands in the longer chain systems is due to the different environments in which the carbon atoms are located along the length of the chain. Between −9 and 0 eV lie the $2p$ bands of N (lowest), C (middle), and O (highest). The hydrogen atoms associated with the carbon and nitrogen atoms contribute their single $1s$ electrons to the bands of their respective atoms.

The oxygen band, from −2 to 0 eV, closely resembles that of the tungsten oxides and bronzes. There is relatively little organic or tungsten component to this band, so once again the valence band is comprised of oxygen $2p$ orbitals. The conduction band begins at around 0.4 eV but the density of states is very low up to a peak feature at about 2.7 eV. There is also a second peak feature at 4.0 eV. This band is comprised mostly of tungsten $5d$ orbitals, as in the tungsten oxides and bronzes, but in these hybrid compounds there is an additional oxygen $2p$ component to this band. The apical oxygen atom contributes to the first peak feature and the planar oxygen atoms contribute to the second. Above 4.5 eV lie the organic antibonding orbitals. The band structure in the vicinity of the Fermi level is virtually identical for the three different organic intercalates, showing that the inorganic layers are essentially decoupled. As expected the organic molecule does not participate in electronic conduction and the compound is an insulator. Peak features in the calculated band structure relate very closely to band gaps as determined by UV-visible spectroscopy.[52] Powder spectra of the hybrids indicate a shift in the absorption edge from 2.6–2.8 eV for WO_3 to 4.1 eV for the hybrids.[18] There was no systematic variation amongst the positions of the absorption edges for the hybrid materials. It appears likely that the features in the UV-visible powder spectra correspond to indirect band gaps, which are displayed in the calculated density of states spectra as peak features in the conduction band, where the dispersion is very flat.

VII. SUMMARY

A number of tungsten oxide-based systems have been studied using *ab initio* computation techniques. Hexagonal and cubic alkali tungsten bronzes exhibit trends in cell sizes which agree well with experimental data. The band structure and charge-density plots of these show that the intercalated alkali atom (with the exception of hydrogen) donates its electron to the conduction band. An in-depth study of the partially doped cubic sodium bronze system showed the progressive movement of the Fermi level into the conduction band. However it is suspected that in the experimental system the onset of metallic conductivity is associated with or induced by a phase change not accounted for in these calculations. A transition to a conducting state is also observed experimentally in oxygen-deficient tungsten trioxide. This is modeled well by the calculations, as are the changing cell dimensions. The free energy indicates that a slight deficit of oxygen renders tungsten trioxide more stable than the exactly stoichiometric form, which is also observed experimentally. Lastly three tungsten-oxide/organic hybrids with simple α,ω-diaminoalkane spacer molecules were studied. They are energetically stable and exhibit many similarities in the band structure to that of the parent cubic tungsten trioxide. The amines are protonated to form ammonium groups and the undoped diammoniumalkane hybrids are calculated to be electrically insulating.

ACKNOWLEDGMENTS

The authors would like to acknowledge financial assistance from the New Zealand Foundation of Research Science and Technology (Contract No. IRLX0201), the Royal Society of New Zealand Marsden Fund, and the MacDiarmid Institute for Advanced Materials and Nanotechnology (Victoria University, New Zealand). We also wish to thank Alan Kaiser for helpful discussions and advice.

[1] M. Figlarz, Prog. Solid State Chem. **19**, 1 (1989).
[2] B. Mourey, M. Hareng, B. Dumont, J. Desseine, and M. Figlarz, *Eurodisplay Proc.* (1984) p. 223.
[3] J. C. Bailar, H. J. Emeleus, R. Nyholm, and A. F. Trotman-Dickenson, eds., *Comprehensive Inorganic Chemistry* (Pergamon, Oxford, 1973), Vol. 4, Chap. 50.
[4] J. D. Guo, K. P. Reis, and M. S. Whittingham, Solid State Ionics **53**, 315 (1992).
[5] A. Coucou and M. Figlarz, Solid State Ionics **28–30**, 1762 (1988).
[6] J. C. Bailar, H. J. Emeleus, R. Nyholm, and A. F. Trotman-Dickenson, eds., *Comprehensive Inorganic Chemistry* (Pergamon, Oxford, 1973), Vol. 3, Chap. 36, p. 623.
[7] S. K. Haydon and D. A. Jefferson, J. Solid State Chem. **168**, 306 (2002).
[8] C. Grenthe and M. Sundberg, J. Solid State Chem. **167**, 402 (2002).
[9] M. E. Straumanis, J. Am. Chem. Soc. **71**, 679 (1949).
[10] W. R. Gardner and G. C. Danielson, Phys. Rev. **93**, 46 (1954).
[11] R. B. Goldner, T. E. Haas, G. Seward, K. K. Wong, P. Norton, G. Foley, G. Berera, G. Wei, S. Schulz, and R. Chapman, Solid State Ionics **28–30**, 1715 (1998).
[12] K. Bange, Sol. Energy Mater. Sol. Cells **58**, 1 (1999).
[13] C. M. Lampert, Sol. Energy Mater. Sol. Cells **52**, 207 (1998).
[14] H. R. Shanks, Solid State Commun. **15**, 753 (1974).
[15] S. H. Lee, H. M. Cheon, C. E. Tracy, A. Mascarenhas, A. W. Czanderna, and S. K. Deb, Appl. Phys. Lett. **75**, 1541 (1999).
[16] A. Georg, W. Graf, and V. Wittwer, Sol. Energy Mater. Sol. Cells **51**, 353 (1998).
[17] O. Glemser and H. Sauer, Z. Anorg. Chem. **252**, 144 (1943).
[18] S. V. Chong, B. Ingham, and J. L. Tallon, Curr. Appl. Phys. **4**, 197 (2004).
[19] B. Ingham, S. V. Chong, and J. L. Tallon, Mater. Res. Soc. Symp. Proc. **775**, 165 (2003).
[20] B. Ingham, S. C. Hendy, S. V. Chong, and J. L. Tallon, physics/0502002 (2005).
[21] A. D. Walkingshaw, N. A. Spaldin, and E. Artacho, Phys. Rev. B **70**, 165110 (2004).
[22] J. P. Perdew, K. Burke, and M. Ernzerhof, Phys. Rev. Lett. **77**, 3865 (1996).
[23] G. Kresse and J. Hafner, Phys. Rev. B **47**, R558 (1993).
[24] G. Kresse, Ph.D. thesis, Technische Univerität Wien, 1993.
[25] G. Kresse and J. Furthmüller, Comput. Mater. Sci. **6**, 15 (1996).
[26] G. Kresse and J. Furthmüller, Phys. Rev. B **54**, 11169 (1996).
[27] D. Vanderbilt, Phys. Rev. B **41**, R7892 (1990).
[28] G. Kresse and J. Hafner, J. Phys.: Condens. Matter **6**, 8245 (1994).
[29] W. Orellana, A. J. R. da Silva, and A. Fazzio, Phys. Rev. Lett. **87**, 155901 (2001).
[30] D. W. Bullett, J. Phys. C **16**, 2197 (1983).
[31] B. W. Brown and E. Banks, J. Am. Chem. Soc. **76**, 963 (1954).
[32] V. M. Goldschmidt, Naturwiss. **14**, 477 (1926).
[33] B. L. Chamberland, Inorg. Chem. **8**, 1183 (1969).
[34] R. S. Roth and J. L. Waring, J. Res. Natl. Bur. Stand., Sect. A **70**, 281 (1966).
[35] O. Glemser and C. Naumann, Z. Anorg. Allg. Chem. **265**, 288 (1951).
[36] G. Aylward and T. Findlay, *SI Chemical Data* (Jacaranda Wiley, Brisbane, 1994).
[37] B. S. Hobbs and A. C. C. Tseung, J. Electrochem. Soc. **119**, 580 (1972).
[38] F. D. Quarto, A. D. Paola, and C. Sunseri, Electrochim. Acta **26**, 1177 (1981).
[39] K. Gesheva, A. Szekeres, and T. Ivanova, Sol. Energy Mater. Sol. Cells **76**, 563 (2003).
[40] L. Ottaviano, F. Bussolotti, L. Lozzi, M. Passacantando, S. L. Rosa, and S. Santucci, Thin Solid Films **436**, 9 (2003).
[41] O. Y. Khyzhun, Y. M. Solonin, and V. D. Dobrovolsky, J. Alloys Compd. **320**, 1 (2001).
[42] A. Hjelm, C. G. Granqvist, and J. M. Wills, Phys. Rev. B **54**, 2436 (1996).
[43] F. Cora, M. G. Stachiotti, and C. R. A. Catlow, J. Phys. Chem. B **101**, 3945 (1997).
[44] B. W. Brown and E. Banks, Phys. Rev. **84**, 609 (1951).

[45] E. O. Brimm, J. C. Brantley, J. H. Lorenz, and M. H. Jellinek, J. Am. Chem. Soc. **73**, 5427 (1951).
[46] G. D. Rieck, *Tungsten and Its Compounds* (Pergamon, Oxford, 1967).
[47] A. Magneli, Ark. Kemi **1**, 513 (1950).
[48] A. Magneli, Ark. Kemi **1**, 223 (1949).
[49] J. Booth, T. Ekstrom, E. Iguchi, and R. Tilley, J. Solid State Chem. **41**, 293 (1982).
[50] J. T. Szymanski and A. C. Roberts, Can. Mineral. **22**, 681 (1984).
[51] D. B. Mitzi, Prog. Inorg. Chem. **48**, 1 (1999).
[52] B. Ingham, S. V. Chong, and J. L. Tallon, Curr. Appl. Phys. **4**, 202 (2004).